

Towards Next Generation Gravitational Wave Detectors: Wavefront Sensing and Mode Matching with the Phase Camera

Yaru Luc^{*}
Pomona College

Advisors: Ricardo Cabrita[†], Morgane Zeoli[‡] and Joris van Heijningen[‡]
(Dated: August 22, 2023)

Third generation gravitational wave detectors face challenges that limited second generation gravitational wave detectors, including reducing seismic noise, quantum noise, and thermal noise, and increasing circulating power. This paper presents two projects that are working to account for these challenges: the (1) Einstein Telescope prototype being assembled at the University of Liège and (2) a phase camera mode mismatch detection setup being worked on at UCLouvain. This paper reports on the UCLouvain project aiming to use a phase camera to measure mode mismatch. The experimental methodologies are presented.

I. INTRODUCTION

In 1916, Einstein predicted the existence of gravitational waves (GWs). In 2015, LIGO detected GWs for the first time directly. Since then, physicists have continued to research ways to make GW detectors more sensitive with techniques like using squeezed light to reduce photon shot noise and increasing laser power. However, while these techniques increase sensitivity, using optical cavities also introduce power losses in GW detectors when they aren't stable or properly aligned. Mode mismatch is a key contributor to optical loss.

We present an optical experiment that will ultimately be used in the 80-meter suspended silicon coupled cavity to mitigate this optical loss. A table-top experiment is under construction and early simple cavity simulations yield the error signals needed.

The presented optical techniques used in the coupled cavity setup at UCLouvain gives us an understanding that can be applied to future developments of GW detectors. Furthermore, our experiment uses a 1550nm laser. Automating mode mismatch control at 1550nm and understanding phase camera mode matching sensing is essential for current and future detectors such as Advanced Virgo (AdV), where two phase cameras^[1] are already installed.

II. MOTIVATIONS

The methods used in this project, like operating at a higher laser wavelength and lower frequency, prepares these techniques for the next generation of GW detectors. The phase camera project will allow researchers to help solve the challenges for the next generation of GW detectors: mode matching at high optical power and at a

different wavelength. Additionally, these techniques can be used in any tabletop setup that uses optical cavities.

A. Limits of 2nd-generation and challenges for 3rd-generation GW detectors

Focusing only on the fundamental noises, the sensitivity of the instruments used in GW detectors is affected by different noises in different frequency ranges, all of which pose challenges that 3rd-generation GW detectors must account for. The sensitivity of the instruments is limited:

1. at very low frequencies (below 4-5 Hz) by seismic noise and the gravity gradient noise. This is because all ground-based detectors are limited at low frequencies by forms of environmental vibration in the soil, from earthquakes to the everyday tectonic shifts in the earth.^[2]
2. in the 4-50 Hz range by thermal noise (like Brownian motion) of the optics suspension system. The two most dominant sources are suspension thermal noise from dissipation in the suspension fibers and thermal noise of the mirror coating.^[4]
3. by forms of quantum noise: radiation pressure noise and shot noise. At low frequencies, this is radiation pressure noise, which comes from the radiation pressure exerted on the suspended mirror by the photons in the main Fabry-Perot cavities. At high frequencies, this is shot noise, which occurs because lasers produce photons randomly. Shot noise can be compared to rainfall: the rate of rainfall, like laser intensity, is measurable, but the raindrops, like photons, fall randomly. This randomness causes fluctuations around the average value, which leads to noise at the output of the detector. Because shot noise is temperature and frequency independent, at high frequencies and low temperatures, shot noise becomes the dominant source of noise.^[2]

* ylac2020@mymail.pomona.edu

† Université Catholique de Louvain

‡ University of Liège

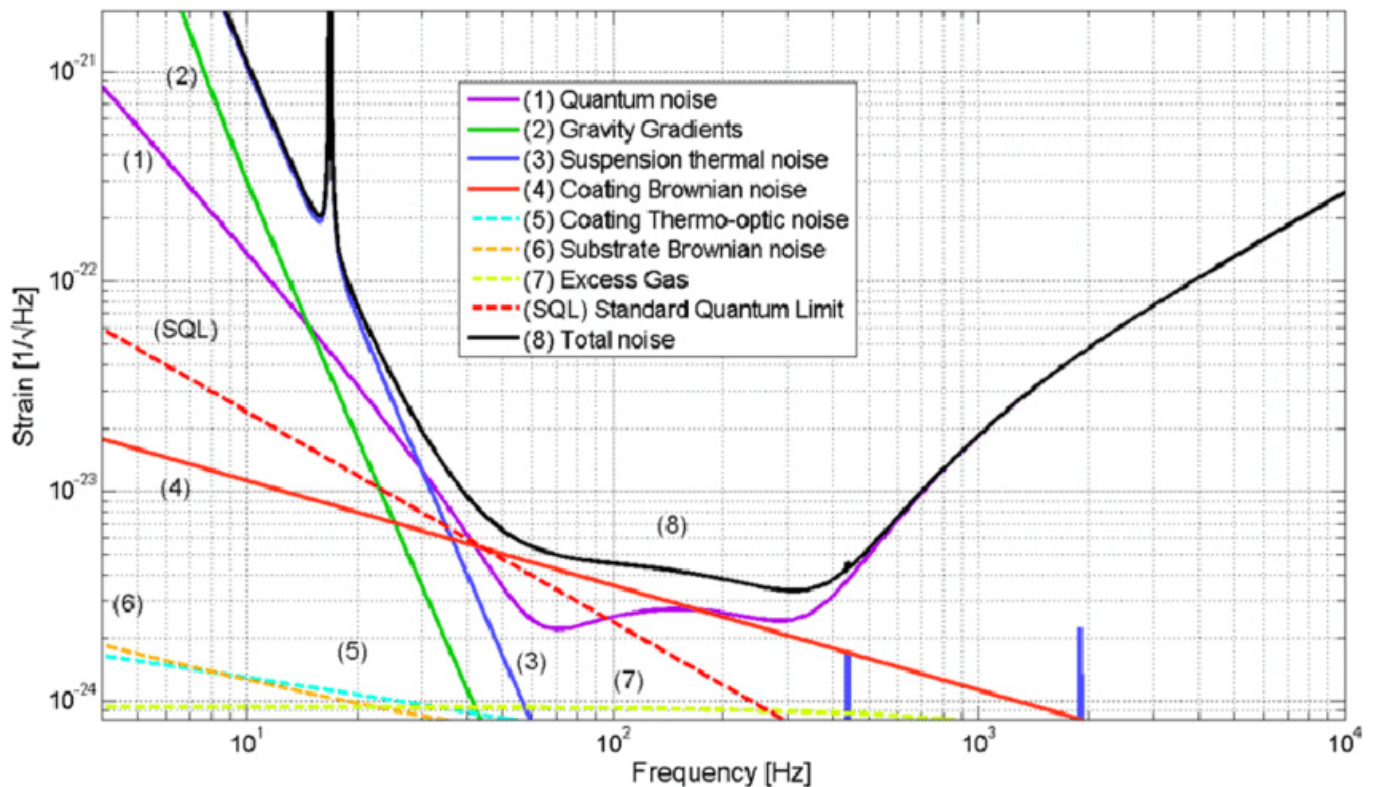


FIG. 1: Retrieved from Cella et. al. [3] The typical sensitivity of a second-generation GW detector (advanced Virgo) is shown here for 125 W of injected power. At low frequencies, sensitivity limitations are dominated by seismic noise and radiation pressure noise, at intermediate frequencies by thermal noise, and at high frequencies by shot noise.

4. by the circulating power in the interferometer. GW signals are generally proportional to the light power inside the interferometer, so increasing power also increases sensitivity of GW detectors. High power in the interferometry arms is achieved in three ways: using high power lasers, power recycling mirrors, or placing Fabry-Perot cavities in the interferometer arms.

Of these four motivations, the ET prototype project at ULiège works to account for the first two. The prototype focuses on optics, low-vibrations cryogenics and seismic isolation. One of the main outcomes of the project will be a full-scale silicon mirror for the Einstein Telescope. [5] Upgrading from ground based mirrors to suspension mirrors greatly mitigates seismic noise, and cooling the end mirrors to cryogenic temperatures near absolute zero and using inertial sensors minimizes thermal noise. [6] The UCLouvain phase camera mode-mismatch project aims to account for the last two.

Furthermore, studies of the Phase Camera (PhC) are motivated by the fact that two are already installed at AdV, so understanding its full potential allows us to use already existing instrumentation. The phase camera has already been studied with GW detectors in initial LIGO, where the infrared (IR) camera was installed next to the optical cavities to monitor the circulating mode shape on the test masses and successfully acquire images of modal

frequency degeneracy. [7]

III. BACKGROUND

A. Mode Mismatch

To set up a Fabry-Perot cavity, two curved mirrors are used. The curvature of those mirrors defines an eigenmode of the cavity, which is the shape of the beam of light that resonates inside the cavity. When a laser is used to illuminate the cavity, the cavity has its own Gaussian beam profile.

Because the beam profile coming out of that laser most likely doesn't match the particular Gaussian beam profile needed inside the cavity for a stable mode, there are a few different things we can do to match the modes. One is to just blast all of the light into the cavity and let the cavity select a portion of that light that matches the mode, but if you do this, you'll get a lot less power resonating in the cavity than is available from the entire laser. This results in power being wasted, so a lens can be placed in front of the cavity along the laser path to try to better match the shape of light going into the cavity to that expected on the inside. But more likely, a pair of lenses would be inserted instead of just one lens, because with a system of lenses, there is an extra degree of free-

dom where you can also control the spacing between the lenses and therefore the focal length to design an optical system where the Gaussian beam profile of light going into the cavity matches the eigenmode of the cavity.^[8] This process is called mode matching, and it is an important step in order to efficiently couple a laser into a cavity.

However, if the input beam of light doesn't match the eigenmode of the cavity, then mode mismatch (MM) occurs. Two types of mode mismatch can occur depending on the waist: waist position and waist size. Position mismatch and size mismatch have different effects on the content of the reflected beam, as one can tell from the two mode mismatch equations^[9]:

$$E_{pos} \propto [\Psi_0 + i \frac{b}{2kw_0^2} (\Psi_0 + \Psi_2)] \quad (1)$$

$$E_{size} \propto [\Psi_0 + \frac{\delta w}{2w_0} \Psi_2] \quad (2)$$

where Ψ_0 and Ψ_2 represent the fundamental and second order modes, $k = \frac{2\pi}{\lambda}$, and w_0 is the nominal cavity eigenmode waist. In equation 1, we see that the position mismatch differs by an i term, so if the phase of the modes in the reflected beam can be detected, then independent information on the waist position and size mismatch can be separated and extracted. The UCLouvain optical setup project aims to use the phase camera (PhC) to address the losses caused by mode mismatch by interpreting this information. By detecting both the size and position mismatch signals with one sensor, we can diagnose, measure, and mitigate thermal noise and mode mismatch.

B. The Phase Camera

The PhC is a frequency selective wavefront imaging sensor. It scans a signal beam over a reference beam

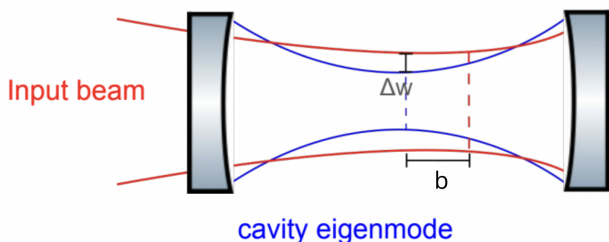


FIG. 2: Retrieved from Ricardo (advisor). The red beam is the eigenmode of the laser input beam and the blue beam is the eigenmode of the cavity. The waist position is mismatched by b and the waist size is mismatched by Δw . Both waist position and waist size mismatches result in increasing optical losses as the mode order is increased.

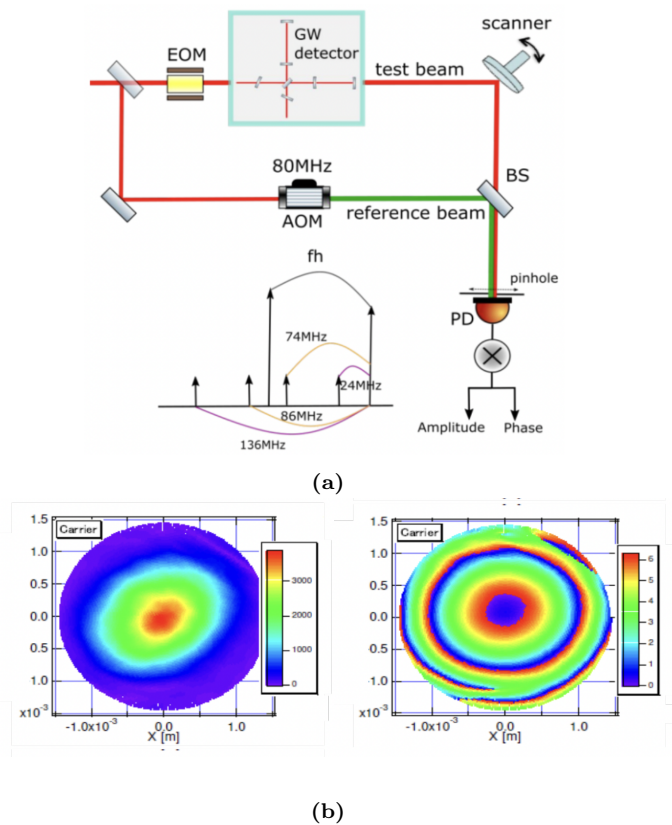


FIG. 3: (a) Retrieved from Ricardo. Phase camera optical schematic. An electro-optic modulator (EOM) is used to introduce sidebands and an acousto-optic modulator (AOM) is used to frequency shift a reference beam (path is shown in green). This reference beam interferes with the test beam (shown in red) at a beam splitter. The interference pattern is read at the photodiode. A heterodyne beat scheme is also shown. (b) Retrieved from Agatsuma et. al. Amplitude (left) and phase (right) images for the carrier frequency.

in order to obtain an interference pattern, similarly to a Mach-Zehnder interferometer. The interference pattern is picked up over a pinhole diode by using a heterodyne technique to analyze sidebands. (A heterodyne technique means that the difference between the signal frequency and carrier frequency is not zero, in contrast to a homodyne technique where there is no difference between the two signals.)

The PhC setup is pictured in Figure 3(a). In this optical schematic, a piezo-scanner is used to scan the test beam and reference beam over the photodiode's pinhole, since the test and reference beams are much larger than the pinhole. An electro-optic modulator (EOM) is used to introduce sidebands and an acousto-optic modulator (AOM) is used to frequency shift a reference beam (path is shown in green). This reference beam interferes with the test beam (shown in red) at a beam splitter. The photodiode reads this interference pattern to allow for demodulation.

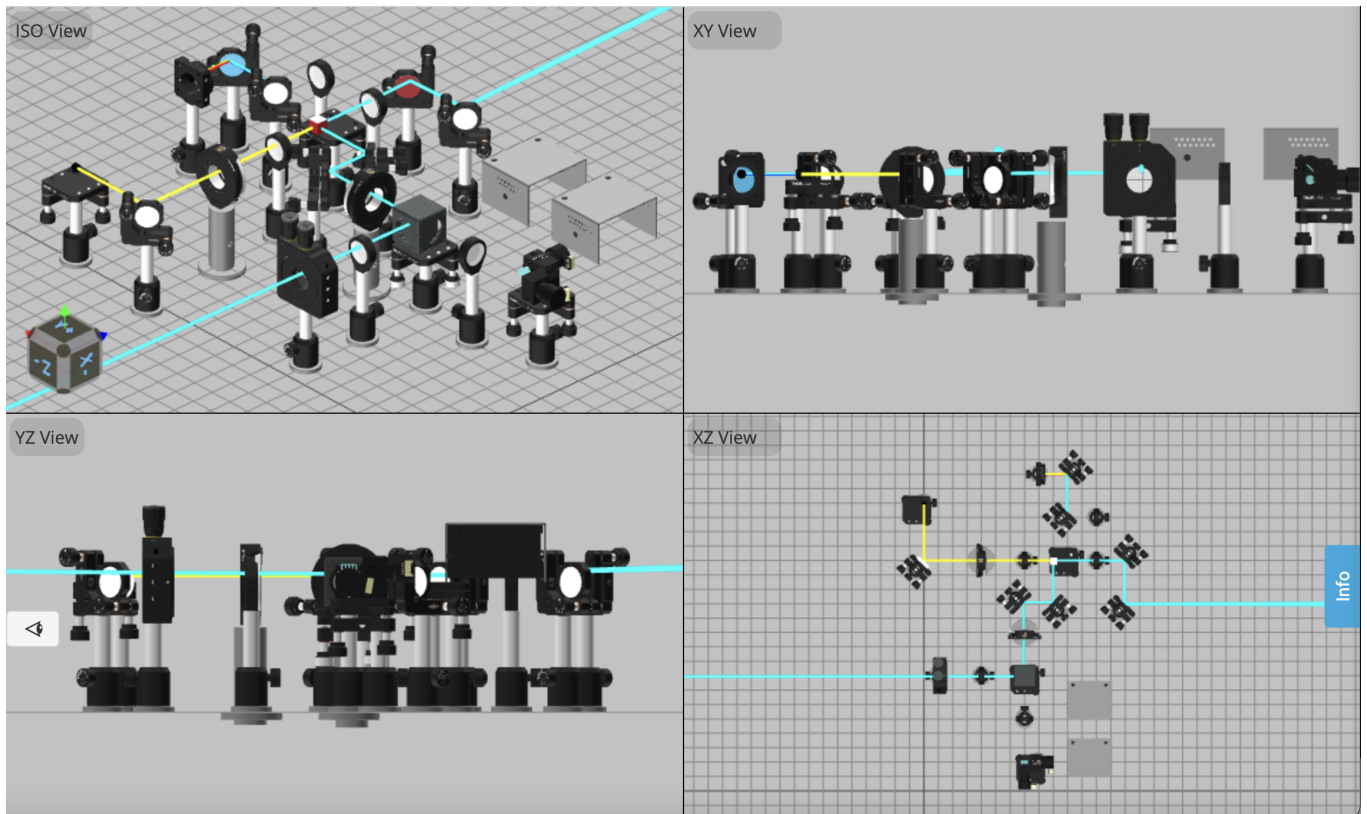


FIG. 4: Designed in 3Doptix. Blue laser beam shows the test beam and yellow shows the beginning of the frequency shifted reference beam (only the optical fibers are shown here, not the laser for the frequency shifted reference beam). Further installations were placed to complete the setup for the frequency shifted reference beam (See Figure 6). The phase camera will detect an interference pattern that occurs when the test beam scans over the reference beam.

The upper and lower sidebands cannot be distinguished without a reference beam. For example, if we look at the heterodyne beat signal in the bottom of Figure 3(a), we could modulate the AOM at 6 MHz to get the smaller signals in the middle. The other sidebands are generated by the EOM. Without a reference beam, the lower and upper sidebands cannot be distinguished from each other since the segments would beat with a carrier (the main frequency) at 6 MHz. With a reference beam, each frequency can be separated since they may beat at 74 MHz and 86 MHz, so you can distinguish the upper from the lower sidebands and also the carrier frequency.

Demodulation occurs when both the amplitude and phase information is extracted. Example amplitude and phase images for the carrier frequencies are shown in Figure 3(b). A piezo scanner is used to acquire a 2D representation of the much larger test and reference beams scanning over the smaller pinhole photodiode.

The goal of this project is to set up the optical schematic of the table shown in Figure 4, and the goal of this summer is to set up the phase camera from Figure 3 into the larger table.

IV. METHODS

A. Phase Camera Work

The number of pixels that the phase camera can show is represented by the equation[1]:

$$L_{sp} = \frac{d_m}{2\sqrt{N}\Delta\theta} * \text{error} \quad (3)$$

where L_{sp} represents the distance from the scanner to the photodiode, N is the number of pixels, and d_m is the image diameter. For more information on this equation, see Appendix A.

The phase camera requires a piezo-scanner to scan the test beam and reference beam over the photodiode's pinhole. We used the Thorlabs GVS012, which is a mirror positioning system designed for custom laser beam steering. The incoming laser beam hits the x-axis mirror and bounces towards the y-axis mirror, and the outgoing laser beam is at a 90 degree angle from the incoming angle, much like a regular optical mirror. Paval, one of the engineers from CP3, and I used Jupyter notebooks for the PFGA programming. With the GVS012, the laser can follow an archimedean spiral pattern (chosen because of

its smooth trajectory to avoid sudden excursions of the mirror and possible overshoots).

Characterization of the resolution of the scanner was required in order to design the PhC setup because this has an impact on the number of pixels of the images. We did this in both the x and y to make sure the laser was not astigmatic, and then used that information to calibrate the plane of the camera.

From the uncertainties, there are two constraints to account for.[1] The first is the fringe separation visibility and the second is the scanner resolution. The first is more strict because it affects the data collection itself, and second is less strict because it is the quality of the retrieval of the data. We took both of these into account to figure out the number of pixels we can set the phase camera to retrieve and find the optical scheme for the reference beam that we arrived at. We found that it needed to be above 0.5 milliradians or 156 DAC steps because we use 30 pixels (since with 30 we get the smallest angle without getting too close to the resolution of the scanner to get errors).

From the scanner resolution uncertainty shown in Figure 6, which was resolved from the piezo-scanner if we allow the laser to stand still, we know that 156 DAC steps is well within the resolution of the scanner. The uncertainty here ranges just from -40 to 40 DAC steps, and 156 DAC steps is much larger than the 80 DAC step uncertainty range.

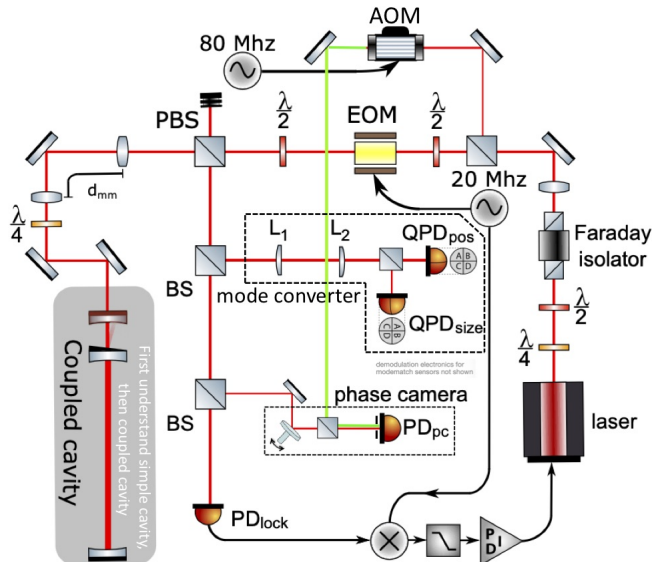


FIG. 5: Retrieved from Joris (advisor). Optical schematic of the full setup of the table. The Phase Camera is shown along with a mode converter, which acts as a benchmark to compare the PhC signals from mode mismatch to.[10]

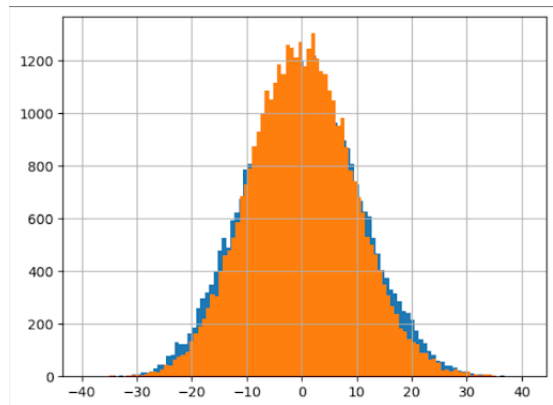


FIG. 6: Scanner resolution uncertainty from calibration of the GVS012 piezo-scanner.

B. Cavity Mode Matching

Recall that mode mismatch can be mitigated by placing two lenses in front of it in order to adjust the focal length of the laser beam image and design an optical system such that the Gaussian beam profile of light going into the cavity matches the eigenmode of the cavity. This summer, we also designed the mode matching telescope for the cavity (shown by the two lenses on the top left separated by d_{mm} in Figure 5) in order to mode match the cavity.

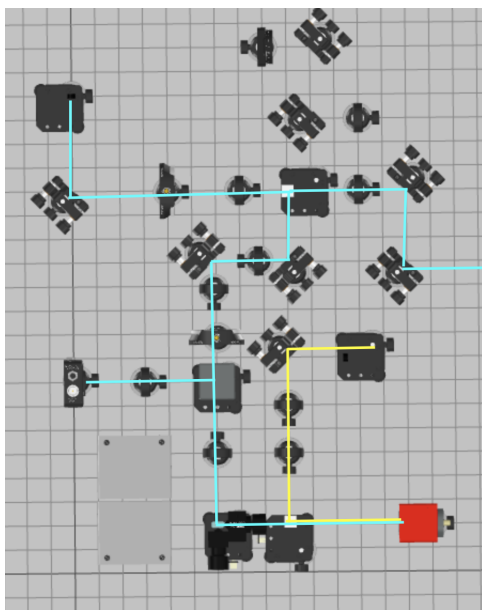
In Figure 8(a), we can see a plot of the cavity scan to confirm this. In the figure, different cavity modes are displayed across one Free Spectral Range (FSR) as we scan the frequency of the laser. This is done by applying a ramp to the laser's current, resulting in an approximately linear scan of the frequency. In this case, the length of the cavity is 0.075 meters. See Appendix B for more information on the FSR.

We are using curved mirrors rather than plane mirrors, so the cavity also acts as a spatial filter (the cavity is doing a physical modal decomposition of the beam we are sending inside). That is to say, we know the cavity expects a specific position and waist size. If you shoot a beam inside the cavity that doesn't match the expected beam, the cavity will force your beam to look like that because of the mirrors are curved (and because of something called the g-factors of the cavity). So the laser can be shaped that way to prevent higher order modes from showing up.

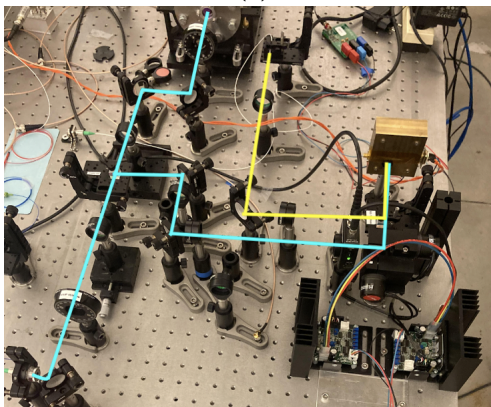
Because we have curved mirrors, different order modes resonate differently (because really the resonance condition depends on the round trip phase acquired, and higher order modes (HOMs) acquire more phase due to more Gouy phase[11] accumulation). These modes appear in a FSR scan separated by the amount:

$$\frac{(\text{mode order})}{\pi} * \arccos\left(\frac{1-L}{RoC}\right) \quad (4)$$

where RoC is the radius of curvature of the mirror.



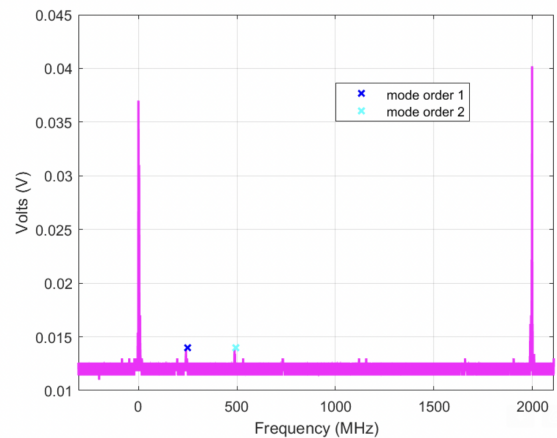
(a)



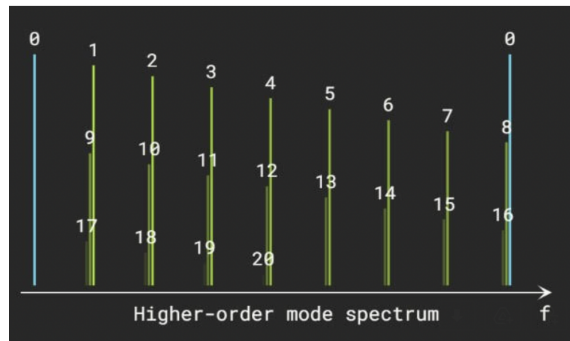
(b)

FIG. 7: (a) Schematic of the full setup of the phase camera. The yellow shows the full path of the frequency shifted reference beam (after being revealed into a laser source from the optical fiber path coming from the AOM, which is shown in Figure 5). The blue shows the path of the test beam. The test beam comes from a laser source, created in-house, on the left of the table image, and exits towards the right of the table image to enter the optical cavity. The test and reference beams interfere with each other at the beam splitter and then enter the phase camera (shown as a red box in the figure) for image retrieval. (b) Photograph of the actual optical table setup is shown, with the same labeled paths.

In Figure 8(b), we can see the mode separation of the cavity, specifically the theoretical position of the first and second order modes superimposed, which fit perfectly well with our measurement in Figure 8(a). From the plot, there should be less than a 5% mode mismatch. 5% is pretty good for eye-balling, and notice that there is also about 5% first order mode. First order modes



(a)



(b)

FIG. 8: (a) Plot of the cavity scan, shown across one Free Spectral Range (FSR). For more information on the FSR, see Appendix B. (b) Theoretical position of modes of order one and two, superimposed with the actual measurements from (a). This diagram from the Linear Cavity Simulator shows accurate mode matching done from our telescope alignment, since there is less than a 5% mode mismatch (calculated by the second mode order divided by the zeroth mode order, and subtracting the noise baseline). Furthermore, since there is about 5% first order mode, if misalignment is improved, the mode mismatching would go down even further.

are because the input light is tilted with respect to the cavity axis, and this misalignment actually couples into mode mismatch (because the beam is tilted and travels longer to cross the cavity, so it screws with the waist position matching). Therefore, this means if we managed to improved the misalignment, the mode matching would probably go down even further – showing the satisfactory success of the telescope for mode matching the cavity.

ACKNOWLEDGMENTS

I wish to acknowledge the generous support of the University of Florida and the IREU team (Prof. Paul Fulda, Dr. Peter Wass, Kathryn, and Nathaniel), as well as the

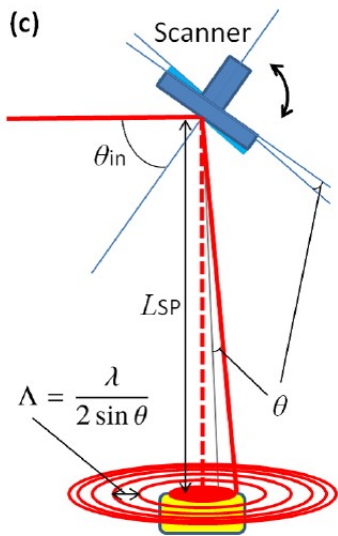


FIG. 9: Retrieved from Agatsuma *et al.* An image showing the definition of angles for L_{sp} . Λ is the spatial fringe gap made by two flat beams with two different incident angles and λ is the wavelength of the laser.

NSF (NSF PHY-1950830) for providing me this incredible opportunity to exercise my curiosity about research in physics and obtain the valuable cultural enrichment that came with living abroad. An especially special gratitude to my three advisors, Ricardo, Morgane, and Joris.

Appendix A: Addendum to Phase Camera L_{sp} equation

Recall that L_{sp} is the distance from the scanner to the photodiode, d_{mm} is the distance between the two

telescopes in front of the photodiode, N is the number of pixels total on the image (we use \sqrt{N} in calculations as it is easier to evaluate the number of rows or columns of pixels rather than the number of pixels itself of an image), and θ is as defined in Figure 9.

Two constraints exist with the phase camera trigonometry conditions: (1) the fringe separation, affecting the lower band, and the (2) scanner resolution, affecting the upper band. The fringe gap must be larger than the active area of the photodiode to detect the heterodyne signals. That is to say:

$$L_{sp} > \frac{d_m * d_{PD}}{\lambda} \quad (A1)$$

where d_{PD} is the pinhole size and d_m is the image diameter of the image at the position of the photodiode. This condition is derived from the relation $\frac{d_m}{2} = L_{sp} * 2\theta$.

The second condition gives us Equation (3) when

$$L_{sp} < \frac{d_m}{\sqrt{N_{\text{pixels}}} \Delta\theta_s} * \text{error} \quad (A2)$$

is satisfied.[1] All of this assumes the photodiode active area is square.

Appendix B: More on the FSR

A cavity's endless resonant frequencies is given by:

$$v = \frac{qc}{2L} \quad (B1)$$

where c is the speed of light, L is the length of the cavity, and q is a unitless integer number for the q^{th} resonating mode of the cavity. Note that $\frac{c}{2L}$ is in frequency units and represents how far away each resonance is in frequency. This is the free spectral range. The FSR only depends on the length of the cavity, and in our case for $L = 0.075$, it is around 2 GHz.

-
- [1] K. Agatsuma *et al.*, High-performance phase camera as a frequency selective laser wavefront sensor for gravitational wave detectors, *Optica* **27**, 18533 (2019).
 - [2] Wikipedia, Gravitational wave observatory: Laser interferometers, https://en.wikipedia.org/wiki/Gravitational-wave_observatory, accessed: 2023-07-23.
 - [3] G. Cella, M. Punturo, *et al.*, The third generation of gravitational wave observatories and their science reach, *Classical and Quantum Gravity* (2010).
 - [4] J. Steinlechner, Development of mirror coatings for gravitational-wave detectors, *Philosophical Transactions: Mathematical, Physical and Engineering Sciences* **376**, 1 (2018).
 - [5] UCLouvain, E-test experiment, <https://uclouvain.be/en/research-institutes/irmp/cp3/e-test.html>, accessed: 2023-08-01.
 - [6] A. Sider, J. Heijningen, *et al.*, E-test: a compact low-frequency isolator for a large cryogenic mirror, *Classical and Quantum Gravity* **40**, 27 (2023).
 - [7] L. K. Agatsuma *et al.*, High-performance phase camera as a frequency selective laser wavefront sensor for gravitational wave detectors, *Opt. Express* **27**, 18533 (2019).
 - [8] Peter Beyersdorf, Mode matching, <https://www.youtube.com/watch?v=5bR6wkZGa18>, published: 21 Aug 2012.
 - [9] E. Morrison *et al.*, Experimental demonstration of an automatic alignment system for optical interferometers, *Optica* **33**, 5037 (1994).
 - [10] F. Magaña-Sandoval *et al.*, Sensing optical cavity mismatch with a mode-converter and quadrant photodiode, *American Physical Society* (2019).
 - [11] S. Feng and H. G. Winful, Physical origin of the gouy phase shift, *Optics Letters* **26** (2001).

- [12] H. Kogelnik and T. Li, Laser beams and resonators, Optica (1966).